

Sharp Interface Limits of the Cahn–Hilliard Equation with Degenerate Mobility

Alpha Albert Lee, Andreas Münch, Endre Süli *

March 2, 2024

Abstract

In this work, the sharp interface limit of the degenerate Cahn–Hilliard equation (in two space dimensions) with a polynomial double well free energy and a quadratic mobility is derived via a matched asymptotic analysis involving exponentially large and small terms and multiple inner layers. In contrast to some results found in the literature, our analysis reveals that the interface motion is driven by a combination of surface diffusion flux proportional to the surface Laplacian of the interface curvature and an additional contribution from nonlinear, porous-medium type bulk diffusion. For higher degenerate mobilities, bulk diffusion is subdominant. The sharp interface models are corroborated by comparing relaxation rates of perturbations to a radially symmetric stationary state with those obtained by the phase field model.

1 Introduction

Phase field models are a common framework to describe the mesoscale kinetics of phase separation and pattern-forming processes [47, 21]. Since phase field models replace a sharp interface by a diffuse order parameter profile, they avoid numerical interface tracking, and are versatile enough to capture topological changes. Although such models can be constructed starting from a systematic coarse-graining of the microscopic Hamiltonian [31, 30, 29, 28], the use as a numerical tool to approximate a specific free boundary problem requires in the first instance careful consideration of their asymptotic long-time sharp interface limits.

In this paper, we will mainly focus on the Cahn–Hilliard equation for a single conserved order parameter $u = u(\mathbf{x}, t)$,

$$u_t = -\nabla \cdot \mathbf{j}, \quad \mathbf{j} = -M(u)\nabla\mu \quad \mu = -\varepsilon^2\nabla^2u + f'(u). \quad (1a)$$

with a double well potential

$$f(u) = (1 - u^2)^2/2 \quad (1b)$$

*Mathematical Institute, University of Oxford, Andrew Wiles Building, Woodstock Road, Oxford, OX2 6GG

and the degenerate, quadratic mobility

$$M(u) = (1 - u^2)_+, \quad (1c)$$

on a bounded two-dimensional domain Ω with boundary conditions

$$\nabla u \cdot \mathbf{n} = 0, \quad \mathbf{j} \cdot \mathbf{n} = 0 \quad (1d)$$

at $\partial\Omega$. Here, $(\cdot)_+$ is the positive part of the quantity in the brackets, \mathbf{x} represents the two-dimensional spatial coordinates, t is the time, μ the chemical potential, \mathbf{j} the flux, and \mathbf{n} the outward pointing normal to $\partial\Omega$. Boldface characters generally represent two-dimensional vectors. Both the potential and the mobility are defined for all u . The mobility is continuous but not differentiable at $u = \pm 1$.

The case of a Cahn-Hilliard equation with a constant mobility has been intensively discussed in the literature. In particular, the sharp interface limit $\varepsilon \rightarrow 0$ was determined by Pego [46], and subsequently proven rigorously by Alikakos et al. [3]. On a long time scale, $t = O(\varepsilon^{-1})$, the result is the Mullins–Sekerka problem [44]. In particular, the motion of the interface between the two phases is driven by flux from bulk diffusion.

In contrast, Cahn-Hilliard equations with degenerate mobility are commonly expected to approximate interface motion by surface diffusion [43] on the time scale $t = O(\varepsilon^{-2})$, where the interface velocity v_n is proportional to the surface Laplacian Δ_s of the interface curvature κ ,

$$v_n \propto \Delta_s \kappa. \quad (2)$$

We note that the surface Laplacian is equal to $\partial_{ss}\kappa$ in two space dimensions, where s is the arclength. In fact, for the case of the degenerate mobility $M(u) = 1 - u^2$ and either the logarithmic free energy

$$f(u) = \frac{1}{2}\theta [(1+u)\ln(1+u) + (1-u)\ln(1-u)] + \frac{1}{2}(1-u^2),$$

with temperature $\theta = O(\varepsilon^\alpha)$, or the double obstacle potential

$$f(u) = 1 - u^2 \quad \text{for } |u| \leq 1, \quad f(u) = \infty \quad \text{otherwise,}$$

Cahn *et al.* [18] showed via asymptotic expansions that the sharp interface limit is indeed interface motion by surface diffusion (2).

Although the logarithmic potential and the double obstacle potential as its deep quench limit are well motivated, in particular for binary alloys, [16, 17, 52, 19, 28, 36, 48, 12], other combinations of potentials and mobility have been used in the literature as a basis for numerical approaches to surface diffusion [20]. Those models are often employed in more complex situations with additional physical effects, such as the electromigration in metals [42], heteroepitaxial growth [49], anisotropic fields [53, 54], phase separation of polymer mixtures [58, 57] and more recently in solid-solid dewetting [34] and coupled fluid flows [2, 51, 1]. In those models, a smooth polynomial double-well free energy is used in combination with the mobility $M(u) = 1 - u^2$ or the degenerate biquadratic mobility

$M(u) = (1 - u^2)^2$ for $|u| \leq 1$. A smooth free energy is numerically more convenient to implement, especially in a multiphysical model, as it avoids the singularity present in either the logarithmic or double obstacle potential. Authors typically justify their choice of mobility and free energy by adapting the asymptotic analysis by Pego [46] and Cahn et al. [18] to obtain the interface motion (2) in the sharp interface limit.

Interestingly, Gugenberger et al. [33], recently revisited some of these models and pointed out an apparent inconsistency that appears in the asymptotic derivations except when the interface is flat. Other evidence suggests that the inconsistency may not be a mere technicality but that some bulk diffusion is present and enters the interfacial mass flux at the same order as surface diffusion. This was observed for example by Bray and Emmott [15] when considering the coarsening rates for dilute mixtures, and by Dai and Du [22] where the mobility is degenerate on one but is constant on the other side of the interface; the papers by Glasner [32] and Lu et al. [41] also use a one-sided degenerate mobility but consider a time regime where all contributions from the side with the degeneracy are dominated by bulk diffusion from the other.) In fact, an early publication by Cahn and Taylor [17] remarked that using a biquadratic potential might not drive the order parameter close enough towards ± 1 to sufficiently suppress bulk diffusion, citing unpublished numerical results. Diffuse interface models for binary fluids with a double well potential and a quadratic mobility $M(u) = 1 - u^2$ or $M(u) = (1 - u^2)_+$ are investigated in [1, 51]. However, in both studies, the leading order expressions for the interface motion do not contain bulk diffusion contributions.

In this paper, we aim to resolve the apparent conundrum in the literature, and revisit the sharp interface limit for (1). We will obtain a sharp interface model where the interface motion is driven by surface diffusion, *i.e.* the surface Laplacian, *and* a flux contribution due to nonlinear bulk diffusion either from one or both sides of the interface, depending on the nature of the solutions for u in the outer regime. The matched asymptotic analysis is rather subtle, and involves the matching of exponentially large and small terms and multiple inner layers.

The paper is organised as follows: Section 2 approximates solutions of (1) which satisfy $|u| \leq 1$; Section 3 considers the asymptotic structure of the radially symmetric stationary state, which demonstrates the matched asymptotic expansion and exponential matching technique in a simpler setting; Section 4 returns to the general 2D time dependent problem; Section 5 briefly discusses the sharp interface limit for a class of solutions with the mobility $M(u) = |1 - u^2|$ where $|u| \leq 1$ is not satisfied, and for the Cahn-Hilliard model with a biquadratic degenerate mobility $M(u) = ((1 - u^2)_+)^2$; Section 6 summarises and concludes the work.

2 Preliminaries

In this paper, we are interested in the behaviour of solutions to (1a) describing a system that has separated into regions where u is close to ± 1 , except for inner layers of width ε between them, and evolve on the typical time for surface diffusion, $t = O(\varepsilon^{-2})$. We thus

rescale time via $\tau = \varepsilon^2 t$, so that the Cahn–Hilliard equation reads

$$\varepsilon^2 \partial_\tau u = \nabla \cdot \mathbf{j}, \quad \mathbf{j} = M(u) \nabla \mu, \quad \mu = -\varepsilon^2 \nabla^2 u + f'(u), \quad (3a)$$

and we keep the boundary conditions on $\partial\Omega$,

$$\nabla u \cdot \mathbf{n} = 0, \quad \mathbf{j} \cdot \mathbf{n} = 0. \quad \text{at } \partial\Omega. \quad (3b)$$

We will denote the subsets where $u > 0$ and $u < 0$ by Ω_+ and Ω_- , respectively, and identify the location of the interface with $u = 0$. Moreover, we assume that Ω_+ is convex unless otherwise stated, and has $O(1)$ curvature everywhere. We will focus on solutions of (3a,b) that satisfy $|u| \leq 1$. The existence of such solutions has been shown by Elliott and Garcke [23].

The general procedure to obtain a description of the interface evolution is then to consider and match expansions of (3a,b), the so-called outer expansions, with inner expansions using appropriate scaled coordinates local to the interface. The approach assumes that the solution of (3a,b) is quasi-stationary *i.e.* close to an equilibrium state. Unfortunately, it is not obvious what the appropriate nearby equilibrium state could be in the situation we consider here. The problem arises because equilibrium solution to (3a,b) with constant μ does not generally satisfy the bound $|u| < 1$ inside of Ω_+ [46].

It is helpful to revisit the standard matched asymptotics procedure for (3a,b) to understand the implications of this observation. Notice that the time derivatives drop out of the lower order outer and inner problems. The leading order inner solution for the double well potential is simply a tanh-profile, which matches with ± 1 in the outer solution; the corresponding leading order chemical potential is zero. To next order, the inner chemical potential is proportional to κ , and this supplies boundary conditions for the chemical potential in the outer problem via matching to be $\mu_1 = c_1 \kappa$. Here, μ_1 denotes the first non-trivial contribution to the chemical potential in the outer expansion, $\mu = \varepsilon \mu_1 + O(\varepsilon^2)$, and c_1 represents a fixed numerical value. It is obtained from a detailed calculation along the lines of section 3, which in fact shows that $c_1 > 0$. It is easy to see from the third equation in (3a) that the outer correction u_1 for $u = \pm 1 + \varepsilon u_1$ is given by $u_1 = \mu_1 / f''(\pm 1)$, thus $u = \pm 1 + c_1 \kappa \varepsilon / 4 + O(\varepsilon^2)$ near the interface. Inside Ω_+ , we therefore have that the outer solution $u > 1$. Notice that we have used that f is smooth at $u = \pm 1$ — for the double obstacle potential, there is no correction to $u = \pm 1$ in the outer problem, see [18].

The resolution to the above conundrum comes from the observation that for a degenerate mobility, slowly evolving solutions can arise from situations other than constant μ once $|u|$ gets close to 1. To obtain an indication of how such solutions evolve, we look at numerical solutions of the radially symmetric version of (3a,b) on the domain $\Omega = \{(x, y); r < 1\}$, where $r = (x^2 + y^2)^{1/2}$, starting with a tanh as initial profile such that $u_{\text{init}}(r) < 1$. The spectral method we used is briefly described in the appendix. The numerical solution at a later stage as shown in Fig. 1 is positive for $r < 0.5$ and negative for $r > 0.5$. Notice while for $r > 0.6$ the solution for u levels out into a flat state that is larger than -1 by an amount of $O(\varepsilon)$, for $r < 0.4$ the solution is much closer to $u = 1$. Closer inspection shows that u has a maximum which approaches $u = 1$, say at $r = r^*$.

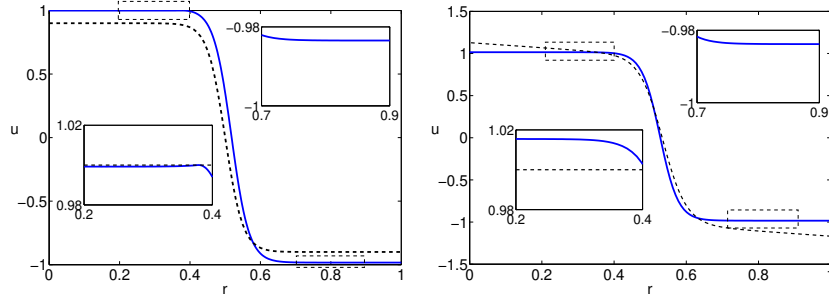


Figure 1: The long-time solution u for the radially symmetric degenerate Cahn–Hilliard equation (1) for different initial data and different mobilities. In (a, left panel), the mobility is (1c) and initial data is bounded within $[-1, 1]$, while in (b, right panel) it exceeds 1 and -1 to the left and right, and the mobility is replaced by $M(u) = |1 - u^2|$, respectively. In both panels, the initial data is shown by dashed lines while the long-time solutions for $\varepsilon = 0.05$ are given by solid lines and have converged close to a stationary state. In (a), this stationary profile is bounded between $[-1, 1]$, where we emphasize that u in the left inset is still below 1 (dashed line in the inset), while in (b), the upper bound 1 is exceeded for r less than about 0.4 (see left inset in (b)). Notice that in both (a) and (b), the value for u for $r > 0.7$ is close to but visibly larger than -1 , by an amount that is consistent with the $O(\varepsilon)$ correction predicted by the asymptotic analysis (for (a) in (18)).

The maximum of u may touch $u = 1$ in either finite or infinite time. In either case, the solution in Ω_+ splits into two parts to the left and right of r^* . The flux between the two parts is very small, and this suggests that they are nearly isolated from each other. In particular, they do not have to be at the same chemical potential. Since we are only interested in the phase field where it determines the evolution of the interface, we cut off the part with $r < r^*$, and consider the remaining part $r > r^*$ as a free boundary problem.

Returning to the general case of not necessarily radially symmetric solutions, we introduce a free boundary Γ near the interface inside Ω_+ , and cut off the parts of the solution further inside of Ω_+ . At Γ , we impose

$$u = 1, \quad \mathbf{n}_\Gamma \cdot \mathbf{j} = 0, \quad \mathbf{n}_\Gamma \cdot \nabla u = 0. \quad (3c)$$

Notice that in addition to $u = 1$ and vanishing normal flux, a third condition has been introduced at Γ . This is expected for non-degenerate fourth order problems and permits a local expansion satisfying (3c) that has the required number of two degrees of freedom [35]. Indeed, expanding the solution to (3) in a travelling wave frame local to Γ with respect to the coordinate η normal to Γ gives $u = 1 - a\eta^2 + O(\eta^3)$, where a and the position of the free boundary implicit in the travelling wave transformation represent the two degrees of freedom.

Also observe that if $u > -1$ by $O(\varepsilon)$ as suggested by the numerical solution in

Fig. 1(a), then $M(u) = O(\varepsilon)$. Since $\mu = O(\varepsilon)$, we expect a nonlinear bulk flux of order $O(\varepsilon^2)$ at the interface arising from Ω_- . This is the same order as the expected flux from surface diffusion. Indeed, as shown below, both contributions are present in the leading order sharp interface model (58d).

Another scenario is conceivable if the mobility is changed to $|1 - u^2|$. Then, with an appropriate initial condition, we obtained numerical results for the radially symmetric case which suggest a solution that is not confined to $|u| < 1$ and which in fact converges to the usual stationary Cahn-Hilliard solution (considered, for example, in [45]) for which μ is constant in Ω , and u is larger than one in most of Ω_+ . These results are shown in Fig. 1(b). In this case, bulk fluxes from both Ω_+ and Ω_- contribute to the leading order interface dynamics, see section 5.1.

3 Radially symmetric stationary solution

By setting $u_\tau = 0$ in (3) for a radially symmetric domain $\Omega = \{(x, y); r < 1\}$ and radially symmetric $u = u(r)$, where $r = (x^2 + y^2)^{1/2}$ and then integrating we obtain

$$\frac{\varepsilon^2}{r} \frac{d}{dr} \left(r \frac{du}{dr} \right) + \eta - 2u(u^2 - 1) = 0, \quad (4a)$$

$$u'(1) = 0, \quad (4b)$$

$$u(r^*) = 1, \quad u'(r^*) = 0. \quad (4c)$$

The point r^* represents the location of the free boundary Γ that needs to be determined as part of the problem. The chemical potential η is constant that needs to be determined by fixing the size of the Ω_+ . This can be done by specifying the $\int_\Omega u$, or, simpler, the position r_0 of the interface,

$$u(r_0) = 0. \quad (4d)$$

Note that if we do not consider a free boundary Γ and impose $u'(0) = 0$ instead of (4c), then there exist exactly two solutions (which can be discerned by the sign of $u(0)$) as was shown in [45]. We will now investigate (4) in the sharp interface limit $\varepsilon \rightarrow 0$ using matched asymptotics. There is one outer region away from the interface, and two inner layers, one located at the interface r_0 and one located at r^* .

Outer region

Inserting the ansatz

$$u = u_0 + \varepsilon u_1 + \cdots, \quad \eta = \eta_0 + \varepsilon \eta_1 + \cdots,$$

into (4a) and (4b) and taking into account that the chemical potential η is a constant quickly reveals that u_0 , u_1 and u_2 are also constants. Their values are fixed by standard matching, that is, they are equal to the limits of the inner solutions as $\rho \rightarrow \infty$, which therefore have to be bounded in this limit.

Inner layer about the interface

To elucidate the asymptotic structure of the interface, we strain the coordinates about r_0 and write

$$\rho = \frac{r - r_0}{\varepsilon}, \quad (5)$$

so that for $U(\rho) = u(r)$, and with the interface curvature $\kappa = 1/r_0$, we have

$$U'' + \varepsilon \frac{U'}{\kappa^{-1} + \varepsilon \rho} + \eta - 2(U^3 - U) = 0, \quad U(0) = 0. \quad (6)$$

Expanding $U = U_0 + \varepsilon U_1 + \dots$, we have, to leading order,

$$U_0'' - 2(U_0^3 - U_0) = \eta_0, \quad U_0(0) = 0. \quad (7)$$

To match with the outer and the solution near Γ , U_0 needs to be bounded for $\rho \rightarrow \pm\infty$, which gives

$$U_0 = -\tanh \rho, \quad \eta_0 = 0. \quad (8)$$

To $O(\varepsilon)$ we have

$$U_1'' - 2(3U_0^2 - 1)U_1 = -\eta_1 - \kappa U_0', \quad U_1(0) = 0, \quad (9)$$

for which the solution that is bounded as $\rho \rightarrow \infty$ is given by

$$\begin{aligned} U_1 = & -\frac{1}{16}(\eta_1 + 2\kappa)\text{sech}^2 \rho + \frac{1}{3}(3\eta_1 - 2\kappa)\text{sech}^2 \rho \left(\frac{3\rho}{8} + \frac{1}{4} \sinh 2\rho + \frac{1}{32} \sinh 4\rho \right) \\ & + \frac{1}{8}(2\kappa - \eta_1) + \frac{1}{48}(2\kappa - 3\eta_1)(2 \cosh 2\rho - 5 \text{sech}^2 \rho). \end{aligned} \quad (10)$$

Inner layer about Γ

We centre the coordinates about the free boundary $r = r^*$ and write

$$z = \rho + \sigma, \quad \sigma \equiv (r_0 - r^*)/\varepsilon. \quad (11)$$

Substituting in the ansatz $\bar{U} = 1 + \varepsilon \bar{U}_1 + \varepsilon^2 \bar{U}_2 + \dots$, we obtain, to $O(\varepsilon)$, the problem

$$\bar{U}_1'' - 4\bar{U}_1 = -\eta_1, \quad (12a)$$

$$\bar{U}_1(0) = 0, \quad \bar{U}_1'(0) = 0, \quad (12b)$$

with the solution

$$\bar{U}_1 = \frac{\eta_1}{4} (1 - \cosh 2z). \quad (13)$$

Matching

We first observe from (4c) that the location of the free boundary Γ in the inner coordinate $\rho = -\sigma$ satisfies $U(-\sigma) = 1$, $U'(-\sigma) = 0$. However, for $\varepsilon \rightarrow 0$, we also have $U \rightarrow U_0 = -\tanh(\rho) < 1$. To reconcile these conditions, we need to assume $\sigma \rightarrow \infty$ as $\varepsilon \rightarrow 0$. Matching of the inner expansions therefore involves exponential terms with large negative arguments ρ , or conversely for large positive z , which we deal with in the spirit of Langer [39], see also [38]. The solution centred at the interface is expanded at $\rho \rightarrow -\infty$ and the result written and re-expanded in terms of $z = \rho + \sigma$. Notice that this change of variables can lead to terms changing their order in ε if σ has the appropriate magnitude. The solution for the layer around the free boundary Γ is directly expanded in terms of $z \rightarrow \infty$ and then the terms are matched between the two expansions.

Expanding U_0 and U_1 for $\rho \rightarrow -\infty$ and substituting $\rho = z - \sigma$ gives

$$\begin{aligned}
 U = & \left(1 - \underbrace{2e^{-2\sigma}e^{2z}}_A + O(e^{4z}) \right) + \varepsilon \left\{ \underbrace{\frac{1}{24}(2\kappa - 3\eta_1)e^{2\sigma}e^{-2z}}_B + \underbrace{\frac{1}{2}(\kappa - \eta_1)}_C \right. \\
 & \left. + \underbrace{\left[\left(\frac{7\eta_1}{4} - \frac{11\kappa}{6} \right) + \left(\frac{3\eta_1}{2} - \kappa \right) (z - \sigma) \right] e^{-2\sigma}e^{2z} + O(e^{4z})}_D \right\} \\
 & + O(\varepsilon^2).
 \end{aligned} \tag{14}$$

The inner expansion for \bar{U} at $z \rightarrow \infty$ is

$$\bar{U} = 1 + \underbrace{\frac{\varepsilon\eta_1}{4}}_E - \underbrace{\frac{\varepsilon\eta_1}{8}e^{2z}}_F - \underbrace{\frac{\varepsilon\eta_1}{8}e^{-2z}}_G + O(\varepsilon^2). \tag{15}$$

Comparing terms in (14) and (15) of the same order of ε functional dependence with respect to z , we notice first that the constant terms at $O(1)$ are already matched. Matching εC and E , yields

$$\eta_1 = \frac{2}{3}\kappa. \tag{16}$$

As a result, the term B is zero. Matching term A and F , we arrive at the condition $2e^{-2\sigma} = \varepsilon\kappa/12$, which we solve for σ , giving

$$\sigma = \frac{1}{2} \log \left(\frac{24}{\varepsilon\kappa} \right). \tag{17}$$

We can now determine the outer solutions. We note that in the more general, time dependent situation, the presence of a non-zero correction will give rise to a flux at $O(\varepsilon^2)$. Using the limits of U_0 and U_1 as $\rho \rightarrow \infty$, we obtain

$$u_0 = -1, \quad u_1 = \frac{\kappa}{6}. \tag{18}$$

Higher corrections

At this stage, it is obvious that the matching is not yet complete to $O(\varepsilon)$, as the terms in (15) and (14), respectively, εD and G are non-zero and lack counterparts in the other expansion. This can be resolved by considering the next higher order solutions \bar{U}_2 and U_2 , which, in fact, will also be useful in section 4. We include $\varepsilon^2 \eta_2$ in the expansion for η , and allow for corrections to σ via the expansion

$$\sigma = \frac{1}{2} \log \left(\frac{24}{\varepsilon \kappa} \right) + \varepsilon \sigma_1 + \dots \quad (19)$$

The $O(\varepsilon^2)$ problem at the interface is given by

$$\begin{aligned} U_2'' - 2(3U_0^2 - 1)U_2 &= -\eta_2 - \kappa U_1' + \rho \kappa^2 U_0' + 6U_0 U_1^2 \\ &= -\eta_2 - \frac{\kappa^2}{6} \tanh^5 \rho - \rho \kappa^2 \operatorname{sech}^2 \rho - \frac{\kappa^2}{3} \tanh \rho \operatorname{sech}^2 \rho, \end{aligned} \quad (20)$$

together with $U_2(0) = 0$ and boundedness for U_2 as $\rho \rightarrow \infty$. The solution is

$$\begin{aligned} U_2 &= -\frac{\eta_2}{8} - \frac{\rho \kappa^2}{4} - \frac{1}{8} \cosh 2\rho \left(\eta_2 + \frac{2}{3} \rho \kappa^2 \right) + \frac{1}{16} \operatorname{sech}^2 \rho \left(5\eta_2 + \frac{23}{6} \rho \kappa^2 - 2\rho^2 \kappa^2 \right) \\ &\quad + \frac{1}{4} \rho \kappa^2 \log \left(\frac{1}{2} e^\rho \right) \operatorname{sech}^2 \rho + \frac{\kappa^2}{8} \operatorname{sech}^2 \rho \operatorname{Li}_2(-e^{2\rho}) \\ &\quad - \frac{\kappa^2}{288} \sinh 2\rho (1 - 24 \log \cosh \rho) \\ &\quad - \frac{\kappa^2}{96} \tanh \rho \left(1 - 24 \log \cosh \rho - \frac{8}{3} \operatorname{sech}^2 \rho \right) + \frac{1}{16} \left(\frac{\pi^2}{6} \kappa^2 - \eta_2 \right) \operatorname{sech}^2 \rho \\ &\quad + \left(\frac{\kappa^2}{36} (1 + 24 \log 2) + \eta_2 \right) \operatorname{sech}^2 \rho \left(\frac{3\rho}{8} + \frac{1}{4} \sinh 2\rho + \frac{1}{32} \sinh 4\rho \right), \end{aligned} \quad (21)$$

where $\operatorname{Li}_2(x)$ is the dilogarithm function.

For $\bar{U}_2(z)$ we have

$$\bar{U}_2'' - 4\bar{U}_2 + \kappa \bar{U}_1' - 6\bar{U}_1^2 + \eta_2 = 0, \quad (22a)$$

$$\bar{U}_2(0) = 0, \quad \bar{U}_2'(0) = 0, \quad (22b)$$

which has the solution

$$\begin{aligned} \bar{U}_2 &= \left(\frac{\kappa}{12} \right)^2 (\cosh 4z + 3e^{-2z}(1 + 4z) - 9) + \left(\frac{\kappa}{12} \right)^2 e^{2z} \\ &\quad + \left(\frac{\kappa}{6} \right)^2 e^{-2z} + \frac{\eta_2}{4} (1 - \cosh 2z). \end{aligned} \quad (23)$$

Expanding $U = U_0 + \varepsilon U_1 + \varepsilon^2 U_2 + \dots$ for $\rho \rightarrow -\infty$, substituting in $\rho = z - \sigma$ and using (19) leads to

$$\begin{aligned} U &= 1 - \frac{\varepsilon \kappa}{12} e^{2z} (1 - 2\varepsilon \sigma_1) + \frac{1}{2} \left(\frac{\varepsilon \kappa}{12} \right)^2 e^{4z} + \varepsilon \left(\frac{\kappa}{6} - \frac{\varepsilon \kappa^2}{36} e^{2z} \right) \\ &\quad + \varepsilon^2 \left[-\frac{1}{8} \eta_2 \left(\frac{24}{\varepsilon \kappa} \right) (1 + 2\varepsilon \sigma_1) e^{-2z} + \left(\frac{\eta_2}{4} - \frac{\kappa^2}{16} \right) \right] + O(\varepsilon^3). \end{aligned} \quad (24)$$

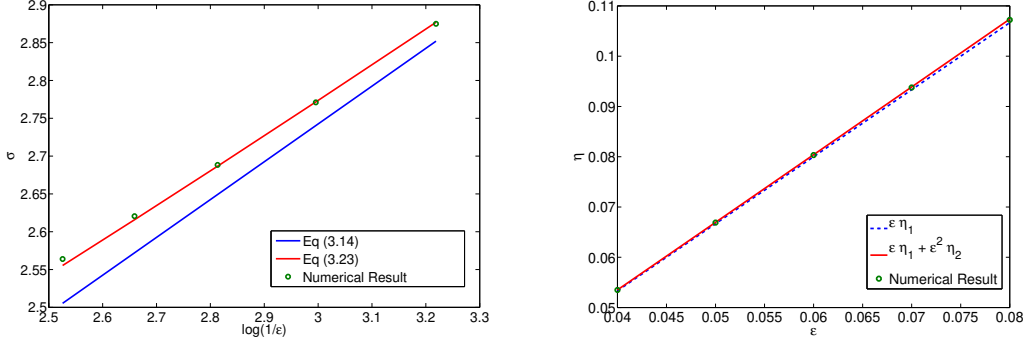


Figure 2: Comparing the asymptotic and numerical results for (left) the position of the free boundary and (right) the chemical potential, for a range of ε and $r_0 = 1/2$.

Similarly, the expansion for $\bar{U} = \bar{U}_0 + \varepsilon \bar{U}_1 + \varepsilon^2 \bar{U}_2 + \dots$ as $z \rightarrow \infty$ is

$$\begin{aligned} \bar{U} = & 1 + \varepsilon \frac{\kappa}{6} (1 - \cosh 2z) \\ & + \varepsilon^2 \left[\frac{1}{2} \left(\frac{\kappa}{12} \right)^2 e^{4z} + \frac{1}{2} \left(\frac{\kappa}{12} \right)^2 e^{-4z} + \left(\frac{\kappa}{12} \right)^2 (3e^{-2z}(1 + 4z) - 9) \right. \\ & \left. + \left(\frac{\kappa}{12} \right)^2 e^{2z} + \left(\frac{\kappa}{6} \right)^2 e^{-2z} + \frac{\eta_2}{4} (1 - \cosh 2z) \right]. \end{aligned} \quad (25)$$

Now, we can match the e^{-2z} at $O(\varepsilon)$ and the e^{2z} at $O(\varepsilon^2)$ terms, and arrive at, respectively,

$$\eta_2 = \frac{\kappa^2}{36}, \quad \sigma_1 = \frac{3\kappa}{16}. \quad (26)$$

For completeness we note that the next order outer correction u_2 is again a constant equal to the limit of U_2 as $\rho \rightarrow \infty$, with the value $u_2 = 7\kappa^2/144$.

Figure 2 shows that the asymptotic results agree well with the position of Γ and the chemical potential obtained from numerical solutions of the ODE free boundary problem (4), confirming the validity of the matched asymptotic results. The solutions were obtained by a shooting method with fixed η using the Matlab package *ode15s*, with $u(1)$ and (4c) as the shooting parameter and condition. The value of η is adjusted in an outer loop via the bisection method until $r_0 = 1/2$ is achieved to a 10^{-10} accuracy.

4 Sharp Interface Dynamics

4.1 Outer variables

Motivated by the stationary state, we now consider the asymptotic structure of the dynamical problem that arises for non-radially symmetric interface geometries. For the

outer expansions, we will use

$$u = u_0 + \varepsilon u_1 + \varepsilon^2 u_2 + \cdots, \quad \mu = \mu_0 + \varepsilon \mu_1 + \varepsilon^2 \mu_2 + \cdots, \quad \mathbf{j} = \mathbf{j}_0 + \varepsilon \mathbf{j}_1 + \varepsilon^2 \mathbf{j}_2 + \cdots.$$

4.2 Inner variables

As in [46, 33], we define the local coordinates relative to the position of the interface (parametrised by s), and write

$$\mathbf{r}(s, r, \tau) = \mathbf{R}(s, \tau) + r \mathbf{n}(s, \tau), \quad (27)$$

where \mathbf{R} , the position of the interface ζ , is defined by

$$u(\mathbf{R}, t) = 0, \quad (28)$$

and $\mathbf{t} = \partial \mathbf{R} / \partial s$ is the unit tangent vector, and \mathbf{n} is the unit outward normal. From the Serret-Frenet formulae in 2D we have that $\kappa \mathbf{t} = \partial \mathbf{n} / \partial s$, thus

$$\frac{\partial \mathbf{r}}{\partial r} = \mathbf{n}(s), \quad \frac{\partial \mathbf{r}}{\partial s} = (1 + r\kappa) \mathbf{t}(s), \quad (29)$$

where $\mathbf{t}(s)$ is the unit tangent vector to the interface, and κ is the curvature. We adopt the convention that the curvature is positively defined if the osculating circle lies inside Ω_+ . The gradient operator in these curvilinear coordinates reads

$$\nabla = \mathbf{n} \partial_r + \frac{1}{1 + r\kappa} \mathbf{t} \partial_s, \quad (30)$$

and the divergence operator of a vector field $\mathbf{A} \equiv A_r \mathbf{n} + A_s \mathbf{t}$ reads

$$\nabla \cdot \mathbf{A} = \frac{1}{1 + r\kappa} \left[\partial_r \left((1 + r\kappa) A_n \right) + \partial_s \left(\frac{1}{1 + r\kappa} A_s \right) \right]. \quad (31)$$

We let s and $\rho = r/\varepsilon$ be the inner coordinates at the interface, and let $U(\rho, s, \tau)$, $\eta(\rho, s, \tau)$ and $\mathbf{J}(\rho, s, \tau)$ denote the order parameter, chemical potential and flux written in these coordinates, respectively. In inner coordinates, the combination of the first two equations, in (3a), and (28), become

$$\varepsilon^2 \partial_\tau U - \varepsilon v_n \partial_\rho U = \nabla \cdot (M(U) \nabla \eta), \quad (32a)$$

$$\eta = -\varepsilon^2 \nabla^2 U + f'(U), \quad (32b)$$

$$U(0) = 0, \quad (32c)$$

with $v_n = \mathbf{R}_\tau \cdot \mathbf{n}$. Using equations (30) and (31), we obtain

$$\begin{aligned}
\nabla \cdot (M(U) \nabla) &= \varepsilon^{-2} \partial_\rho M(U_0) \partial_\rho \\
&+ \varepsilon^{-1} \left\{ \partial_\rho \left(\kappa \rho M(U_0) + M'(U_0) U_1 \right) \partial_\rho - \kappa \rho \partial_\rho M(U_0) \partial_\rho \right\} \\
&+ \left\{ \kappa^2 \rho^2 \partial_\rho M(U_0) \partial_\rho - \kappa \rho \partial_\rho \left(\kappa \rho M(U_0) + M'(U_0) U_1 \right) \partial_\rho \right. \\
&+ \partial_\rho \left(\kappa \rho M'(U_0) U_1 + \frac{1}{2} M''(U_0) U_1^2 + M'(U_0) U_2 \right) \partial_\rho \\
&\left. + \partial_s M(U_0) \partial_s \right\} + O(\varepsilon). \tag{32d}
\end{aligned}$$

Notice that the corresponding expression for ∇^2 can be easily obtained from this by setting $M \equiv 1$.

Taking only the first equation in (3a) we have

$$\varepsilon^2 \partial_\tau U - \varepsilon v_n \partial_\rho U = \frac{1}{1 + \varepsilon \rho \kappa} \left[\varepsilon^{-1} \partial_\rho \left((1 + \varepsilon \rho \kappa) J_n \right) + \partial_s \left(\frac{1}{1 + \varepsilon \rho \kappa} J_s \right) \right]. \tag{33}$$

In inner coordinates, we will only need to know the normal component $J_n = \mathbf{n} \cdot \mathbf{J}$ of the flux explicitly in terms of the order parameter and chemical potential. It is given by

$$\begin{aligned}
J_n &= \frac{M(U)}{\varepsilon} \partial_\rho \eta \\
&= \varepsilon^{-1} M(U_0) \partial_\rho \eta_0 + M'(U_0) U_1 \partial_\rho \eta_0 + M(U_0) \partial_\rho \eta_1 \\
&+ \varepsilon \left(M(U_0) \partial_\rho \eta_2 + M'(U_0) U_1 \partial_\rho \eta_1 + M'(U_0) U_2 \partial_\rho \eta_0 + \frac{1}{2} M''(U_0) U_1^2 \partial_\rho \eta_0 \right) \\
&+ \varepsilon^2 \left[M(U_0) \partial_\rho \eta_3 + M'(U_0) U_1 \partial_\rho \eta_2 + \left(M'(U_0) U_2 + \frac{1}{2} M''(U_0) U_1^2 \right) \partial_\rho \eta_1 \right. \\
&\quad \left. + \left(M'(U_0) U_3 + M''(U_0) U_1 U_2 + \frac{1}{6} M'''(U_0) U_1^3 \right) \partial_\rho \eta_0 \right] + O(\varepsilon^3), \tag{34}
\end{aligned}$$

which also motivates our ansatz for the expansion for \mathbf{J} , given the obvious ansatz for the other variables,

$$\begin{aligned}
U &= U_0 + \varepsilon U_1 + \varepsilon^2 U_2 + \cdots, \quad \eta = \eta_0 + \varepsilon \eta_1 + \varepsilon^2 \eta_2 + \cdots, \\
\mathbf{J} &= \varepsilon^{-1} \mathbf{J}_{-1} + \mathbf{J}_0 + \varepsilon \mathbf{J}_1 + \varepsilon^2 \mathbf{J}_2 + \cdots.
\end{aligned}$$

Moreover, we introduce $z = \rho + \sigma(s, t)$ as the coordinate for the inner layer about the free boundary Γ , so that the order parameter, chemical potential and flux in these variables are given by $\bar{U}(z, s, \tau)$, $\bar{\eta}(z, s, \tau)$ and $\bar{\mathbf{J}}(z, s, \tau)$, respectively, with expansions

$$\begin{aligned}
\bar{U} &= \bar{U}_0 + \varepsilon \bar{U}_1 + \varepsilon^2 \bar{U}_2 + \cdots, \quad \bar{\eta} = \bar{\eta}_0 + \varepsilon \bar{\eta}_1 + \varepsilon^2 \bar{\eta}_2 + \cdots, \\
\bar{\mathbf{J}} &= \varepsilon^{-1} \bar{\mathbf{J}}_{-1} + \bar{\mathbf{J}}_0 + \varepsilon \bar{\mathbf{J}}_1 + \varepsilon^2 \bar{\mathbf{J}}_2 + \cdots.
\end{aligned}$$

Notice that the location where the two inner layers are centred depends on ε and therefore, in principle, σ and also R need to be expanded in terms of ε as well. However, we are only interested in the leading order interface motion, so to keep the notation simple, we do not distinguish between σ and R and their leading order contributions. We now solve and match the outer and inner problems order by order.

4.3 Matching

Leading order

For the outer problem, we obtain to leading order

$$\nabla \cdot \mathbf{j}_0 = 0, \quad \mathbf{j}_0 = M(u_0) \nabla \mu_0, \quad \mu_0 = f'(u_0). \quad (35)$$

The requisite boundary conditions are $\nabla_n u_0 = 0$, and $\mathbf{n} \cdot \mathbf{j}_0 = 0$ on $\partial\Omega$. We have

$$u_0 = -1, \quad \mu_0 = 0. \quad (36)$$

The leading order expansion about the interface reads,

$$M(U_0) \partial_\rho \eta_0 = a_1(s, \tau), \quad f'(U_0) - \partial_{\rho\rho} U_0 = \eta_0. \quad (37)$$

From the matching conditions, we require U_0 to be bounded for $\rho \rightarrow \pm\infty$. In fact, $U(\rho \rightarrow -\infty) = -1$, giving $\eta_0 \rightarrow 0$. This implies $a_1 = 0$, therefore also $\eta_0 = 0$, which we note matches with μ_0 . Moreover, from (37)₂ and from (34) we have

$$U_0 = -\tanh \rho, \quad J_{n,-1} = 0. \quad (38)$$

The leading order approximation of the order parameter in the coordinates of the inner layer at Γ is easily found to be $\bar{U}_0 = 1$, and also for the chemical potential $\bar{\eta}_0 = 0$, and the normal component of the flux $\bar{J}_{n,-1} = 0$.

$\mathcal{O}(\varepsilon)$ correction

The first two parts of the outer correction problem for (3a) are automatically satisfied, since $\mu_0 = 0$ and $M(u_0) = 0$, by

$$\mathbf{j}_1 = 0. \quad (39)$$

The last part requires

$$\mu_1 = f''(u_0) u_1 = 4u_1. \quad (40)$$

From (32), and noting that $\eta_0 = 0$, we have

$$\partial_\rho (M(U_0) \partial_\rho \eta_1) = 0, \quad \eta_1 = -\partial_{\rho\rho} U_1 - \kappa \partial_\rho U_0 + f''(U_0) U_1, \quad U_1(0) = 0, \quad (41)$$

thus $M(U_0) \partial_\rho \eta_1 = J_{n,0}$ is constant in ρ . Since $J_{n,0}$ has to match with j_0 , it is zero. Therefore, $\eta_1 = \eta_1(s, t)$ does not depend on ρ . Now (41)₂ and (41)₃ represent the same problem as (9). As such, the solution $U_1(\rho, s, \tau)$ that is bounded as $\rho \rightarrow \infty$ can be read off (10).

The $O(\varepsilon)$ problem for the inner layer at Γ becomes

$$\bar{\eta}_1 = -\partial_{zz}\bar{U}_1 + 4\bar{U}_1, \quad (42)$$

with $\bar{\eta}_1$ that does not depend on z , supplemented with the conditions $\bar{U}_1(z, 0, \tau) = 1$, $\bar{U}_{1z}(z, 0, \tau) = 0$. This equation is the same as the $O(\varepsilon)$ equation for the stationary state about the free boundary, and the solution is given by (13). The inner layers about Γ and about the interface can be matched, as outlined in section 3, to obtain

$$\bar{\eta}_1 = \eta_1 = \frac{2}{3}\kappa. \quad (43)$$

$O(\varepsilon^2)$ correction

Combining the first two equations in (3a) and expanding to $O(\varepsilon^2)$ yields

$$\nabla \cdot (M'(u_0)u_1\nabla\mu_1) = 0. \quad (44)$$

In view of the discontinuous derivative of M at $u = u_0 = -1$, we remark that here and in the following we will use the convention that $M'(\pm 1)$ denotes the one-sided limit for $|u| \rightarrow 1^-$, in particular that $M'(-1) = 2$, and likewise for higher derivatives. Equation (40) provides a relation between μ_1 and u_1 . Thus, we have

$$\nabla \cdot (\mu_1\nabla\mu_1) = 0 \quad (45)$$

with the boundary condition $\nabla_n\mu_1 = 0$ on $\partial\Omega$, and, from matching μ_1 with η_1 (given in (43)) at the interface,

$$\mu_1 = \frac{2}{3}\kappa. \quad (46)$$

Expanding the second equation in (3a) to $O(\varepsilon^2)$ also gives us an expression for the normal flux

$$\mathbf{n} \cdot \mathbf{j}_2 = u_1 M'(u_0) \nabla_n \mu_1 = \frac{1}{2} \mu_1 \nabla_n \mu_1, \quad (47)$$

which is not in general zero.

Inner expansion about the interface

From the $O(1)$ terms in (32), we obtain

$$\partial_\rho (M(U_0)\partial_\rho\eta_2) = 0. \quad (48)$$

Thus, $M(U_0)\partial_\rho\eta_2$ is constant in ρ and since we can identify this expression via (34) as $J_{n,1}$, which has to match with $\mathbf{n} \cdot \mathbf{j}_1 = 0$. Therefore we can deduce that

$$J_{n,1} = M(U_0)\partial_\rho\eta_2 = 0, \quad (49)$$

and η_2 is independent of ρ . The solution for η_2 is found in essentially the same way as in Section 3, see (19) – (26), thus

$$\eta_2(s, \tau) = \frac{\kappa^2}{36}. \quad (50)$$

$O(\varepsilon^3)$ correction

Noting that η_0 , η_1 and η_2 are independent of ρ , the $O(\varepsilon)$ terms in (32) yield

$$-v_n \partial_\rho U_0 = \partial_\rho M(U_0) \partial_\rho \eta_3 + \frac{2}{3} M(U_0) \partial_{ss} \kappa. \quad (51)$$

Integrating equation (51) from $-\infty$ to ∞ , we arrive at

$$v_n = \frac{1}{2} [M(U_0) \partial_\rho \eta_3]_{-\infty}^{\infty} + \frac{2}{3} \partial_{ss} \kappa. \quad (52)$$

From (34), we can identify the term in the bracket as

$$J_{n,2} = M(U_0) \partial_\rho \eta_3. \quad (53)$$

At $\rho \rightarrow -\infty$, we need to match η_3 and $J_{n,2}$ with the solution for $\bar{\eta}_3$ and $\mathbf{n} \cdot \bar{\mathbf{J}}_2$ in the inner layer at Γ , which in the former case is a function independent of z , and in the latter is just zero. Thus, η_3 is matched to a constant for $\rho \rightarrow -\infty$, and $J_{n,2}$ is matched to zero, thus

$$\lim_{\rho \rightarrow -\infty} M(U_0) \partial_\rho \eta_3 = \lim_{\rho \rightarrow -\infty} J_{n,2} = 0. \quad (54)$$

We next consider the contribution from $J_{n,2}$ as $\rho \rightarrow \infty$. It is tempting to use (53) to argue that, since $M(U_0) \rightarrow 0$ exponentially fast, $J_{n,2}$ also has to tend to zero. Then, however, $J_{n,2}$ cannot be matched with $\mathbf{n} \cdot \mathbf{j}_2$, as we cannot simply set the latter to zero: The bulk equation (45) has already got a boundary condition at ζ , namely (46), and setting $\mathbf{n} \cdot \mathbf{j}_2 = 0$ would impose too many conditions there. We therefore drop the idea that $J_{n,2} \rightarrow 0$ as $\rho \rightarrow \infty$ and match the normal fluxes,

$$\lim_{\rho \rightarrow \infty} J_{n,2} = \mathbf{n} \cdot \mathbf{j}_2|_\zeta, \quad (55)$$

Keeping in mind that non-trivial solutions for μ_1 will arise from (45), (46) and $\nabla_n \mu_1 = 0$ at $\partial\Omega$, we expect that $J_{n,2}$ will not, in general be zero because of (47) and (55). Substituting (53) and (47) into the left and right hand sides of (55), respectively, we obtain

$$\lim_{\rho \rightarrow \infty} M(U_0) \partial_\rho \eta_3 = \frac{1}{2} \mu_1 \nabla_n \mu_1|_\zeta, \quad (56)$$

so that now the boundary terms in (52) have been determined in terms of μ_1 . Now, however, we have to accept that in general there will be exponential growth in η_3 as $\rho \rightarrow \infty$: if the left hand side of (56) is nonzero, and $M(U_0) \rightarrow 0$ exponentially fast as $\rho \rightarrow \infty$, then η_3 has to grow exponentially. In fact, if we solve (53) for η_3 , and eliminate $J_{n,2}$ via (55) and (47), we obtain the solution

$$\eta_3 = \frac{\mu_1 \nabla_n \mu_1|_\zeta}{16} (e^{2\rho} + 2\rho) + \eta_3^0, \quad (57)$$

where η_3^0 is an integration constant. The term proportional $e^{2\rho}$ is the exponentially growing term and it does not appear to be matchable to the outer solution. We will resolve this issue in a separate section, by introducing another inner layer, and for now continue with analysing the sharp interface model, which in summary is given by

$$\nabla \cdot (\mu_1 \nabla \mu_1) = 0, \quad \text{in } \Omega_+, \quad (58a)$$

$$\mu_1 = \frac{2}{3}\kappa, \quad \text{on } \zeta, \quad (58b)$$

$$\nabla_n \mu_1 = 0, \quad \text{on } \partial\Omega_{\text{ext}}, \quad (58c)$$

$$v_n = \frac{2}{3}\partial_{ss}\kappa + \frac{1}{4}\mu_1 \nabla_n \mu_1 \quad \text{on } \zeta. \quad (58d)$$

4.4 Additional inner layer

The exponential growth of η_3 at $\rho \rightarrow \infty$ is a direct consequence of the exponential decay of $M(U_0)$ to 0 as U_0 approaches -1 exponentially fast. Notice, however, that the inner solution including the correction terms does not decay to -1 , because $U_1(\rho \rightarrow \infty) > 0$, so that

$$M(U_0 + \varepsilon U_1 + \dots) = M(U_0) + \varepsilon M'(U_0)U_1 + \dots$$

approaches a non-zero $O(\varepsilon)$ value as $\rho \rightarrow \infty$. We need to ensure that the correction $\varepsilon M'(U_0)U_1$ to $M(U_0)$ enters into the calculation of the chemical potential as soon as ρ is in the range where $M(U_0)$ and $\varepsilon M'(U_0)U_1$ have the same order of magnitude. This happens when $U_0 + 1 = O(\varepsilon)$, i.e. when $\rho \sim -(1/2)\ln \varepsilon$. We therefore introduce another layer via

$$\rho = \frac{1}{2}\ln\left(\frac{1}{\varepsilon}\right) + y, \quad \hat{U}(y) = U(\rho), \quad \hat{\eta}(y) = \eta(\rho), \quad \hat{\mathbf{J}}(y) = \mathbf{J}(\rho).$$

Notice the similarity with the change of variables at Γ . Indeed, the solution in the new layer will have exponential terms in the expansion at $y \rightarrow -\infty$ that need to be matched with the expansion at the interface $\rho \rightarrow \infty$. In terms of the new variables, the Cahn–Hilliard equation becomes

$$\varepsilon^2 \partial_\tau \hat{U} - \varepsilon v_n \partial_y \hat{U} = \nabla \cdot \left(M(\hat{U}) \nabla \hat{\eta} \right), \quad (59)$$

$$\begin{aligned} \hat{\eta} = & -\partial_{yy} \hat{U} - \frac{\varepsilon \kappa}{1 + \varepsilon \kappa \left(y - \frac{1}{2} \ln \varepsilon \right)} \partial_y \hat{U} \\ & - \frac{\varepsilon^2}{1 + \varepsilon \kappa \left(y - \frac{1}{2} \ln \varepsilon \right)} \partial_s \left(\frac{\partial_s \hat{U}}{1 + \varepsilon \kappa \left(y - \frac{1}{2} \ln \varepsilon \right)} \right) + f'(\hat{U}). \end{aligned} \quad (60)$$

We expand

$$\begin{aligned} \hat{U} = & -1 + \varepsilon \hat{U}_1 + \varepsilon^2 \hat{U}_2 + \dots, \quad \hat{\eta} = \varepsilon \hat{\eta}_1 + \varepsilon^2 \hat{\eta}_2 + \dots, \\ \hat{\mathbf{J}} = & \hat{\mathbf{J}}_0 + \varepsilon \hat{\mathbf{J}}_1 + \varepsilon^2 \hat{\mathbf{J}}_2 + \dots, \end{aligned}$$

where we have tacitly anticipated that $\hat{\eta}_0 = 0$, $\hat{\mathbf{J}}_{-1} = 0$. Inserting these gives

$$\nabla \cdot (M(\hat{U})\nabla \hat{\eta}) = \partial_y [M'(-1)\hat{U}_1\partial_y \hat{\eta}_1] + \varepsilon \partial_y [M'(-1)\hat{U}_1\partial_y \hat{\eta}_2] + O(\varepsilon^2). \quad (61)$$

The normal flux $\hat{J}_n = \mathbf{n} \cdot \hat{\mathbf{J}}$ is given by

$$\begin{aligned} \hat{J}_n = \frac{M(U)}{\varepsilon} \partial_\rho \eta &= \left[M'(-1)\hat{U}_1 + \varepsilon \left((M''(-1)/2) \hat{U}_1^2 + M'(-1)\hat{U}_2 \right) + O(\varepsilon^2) \right] \\ &\times [\varepsilon \partial_y \hat{\eta}_1 + \varepsilon^2 \partial_y \hat{\eta}_2 + O(\varepsilon^3)]. \end{aligned} \quad (62)$$

Comparison with the ansatz for the expansion of $\hat{\mathbf{J}}$ immediately implies $\hat{J}_{n,0} = 0$.

Leading order problem

To leading order, we have

$$-\partial_y [M'(-1)\hat{U}_1\partial_y \hat{\eta}_1] = 0, \quad -\partial_{yy} \hat{U}_1 + f''(-1)\hat{U}_1 = \hat{\eta}_1. \quad (63)$$

Integrating the first of these once, we obtain that the expression in square bracket has to be a constant in y . From (62), we see this is the term $\hat{J}_{n,1}$ in the normal flux, which has to match to $J_{n,1}$ and $\mathbf{n} \cdot \mathbf{j}_1$ in the interface layer and the outer problem, respectively. Thus $\hat{J}_{n,1} = 0$. Therefore, the contribution $\hat{\eta}_1$ is also a constant that needs to match to the same value $\kappa/6$ towards the outer and the interface layer, *i.e.* for $\hat{y} \rightarrow \pm\infty$, so that we have

$$\hat{\eta}_1 = \frac{2}{3}\kappa, \quad \hat{U}_1 = c_1 e^{-2y} + c_2 e^{2y} + \frac{1}{6}\kappa. \quad (64)$$

Matching this to the constant outer $u_1 = \kappa/6$, obtained from (40) and (43), forces $c_2 = 0$. We next expand U_0 at $\rho \rightarrow \infty$,

$$U_0 = -1 + 2e^{-2\rho} + O(e^{-4\rho}). \quad (65)$$

The second term accrues a factor of ε upon passing to y -variables, and thus has to match with the exponential term in $\varepsilon \hat{U}_1$, giving $c_1 = 2$ and

$$\hat{U}_1 = 2e^{-2y} + \frac{1}{6}\kappa. \quad (66)$$

First correction problem

To next order, we obtain

$$-\partial_y [M'(-1)\hat{U}_1\partial_y \hat{\eta}_2] = 0, \quad (67a)$$

$$-\partial_{yy} \hat{U}_2 - \kappa \partial_y \hat{U}_1 + f''(-1)\hat{U}_2 + f'''(-1)\hat{U}_1 = \hat{\eta}_2, \quad (67b)$$

$$\hat{J}_{n,2} = M'(-1)\hat{U}_1\partial_y \hat{\eta}_2. \quad (67c)$$

ε	0.01	0.005	0.003	0.002	0.001	Eq (72)	Eq (71)
$\lambda_{m=2}$	-133.2	-133.8	-136.0	-136.3	-137.0	-137.4	-128

Table 1: Relaxation rates obtained from the linearised phase field model (73) are shown for different values of ε in the first five columns, and compared to the eigenvalues obtained for linearised sharp interface models for pure surface diffusion (71) and the porous medium type model (72) in the next-to-last and the last column, respectively, with $\mathfrak{M} = 2/3$.

From (67a) and (67c), and matching the flux contribution $\hat{J}_{n,2}$ to the outer $\mathbf{n} \cdot \mathbf{j}_2$, we obtain

$$M'(-1)\hat{U}_1\partial_y\hat{\eta}_2 = \frac{1}{2}\mu_1\nabla_n\mu_1|_\zeta, \quad (68)$$

which in turn has the solution

$$\hat{\eta}_2 = \frac{\mu_1\nabla_n\mu_1|_\zeta}{\kappa M'(-1)} \ln\left(\frac{\kappa}{12}e^{2y} + 1\right) + \frac{\kappa^2}{36}. \quad (69)$$

The integration constant has been fixed by matching $\hat{\eta}_2$ for $y \rightarrow -\infty$ with the interface solution η_2 , see (50). We now need to check if the exponential term in (69) matches with the exponential term in (57). Expanding at $y \rightarrow -\infty$ is trivial, and then substituting in $y = \rho + \ln \varepsilon/2$ gives

$$\hat{\eta}_2 = \frac{\varepsilon}{8M'(-1)}\mu_1\nabla_n\mu_1|_\zeta e^{2\rho} + \frac{\kappa^2}{36}. \quad (70)$$

Thus, $\varepsilon^2\hat{\eta}_2$ contains a term proportional to ε^3e^{2y} term that is identical to the ε^3e^{2y} term that appears in $\varepsilon^3\eta_3$, see (57). Thus, we have resolved the issue with the exponentially growing term (for $\rho \rightarrow \infty$) in the correction to the chemical potential in the interface layer expansion.

4.5 Linear stability analysis

Besides the usual surface diffusion term, equation (58) contains an additional normal flux term which is nonlocal. In cases where there are multiple regions of u close to 1, the nonlocal term couples the interfaces of these regions with each other and drive coarsening where the larger regions grow at the expense of smaller ones. This is not expected for pure surface diffusion. Even for a single convex domain that is slightly perturbed from its radially symmetric state, the effect on the relaxation dynamics is noticeable, as we now explore.

To compare the sharp interface model with the phase field model, we consider the relaxation of an azimuthal perturbation to a radially symmetric stationary state with curvature $\kappa = 1/r_0$. For azimuthal perturbations proportional to $\cos m\theta$, the pure surface diffusion model $v_n = \mathfrak{M}\partial_{ss}\kappa$ predicts an exponential decay rate

$$\lambda = -\mathfrak{M}\frac{m^2(m^2 - 1)}{r_0^4}. \quad (71)$$

In contrast, the decay rate in the porous medium model, Equation (58), is given by

$$\lambda = -\frac{2}{3} \frac{m^2(m^2 - 1)}{r_0^4} - \frac{1}{9} \frac{m(m^2 - 1)}{r_0^4} \tanh(m \log r_0^{-1}). \quad (72)$$

In the diffuse interface model, the perturbation $v_1(r, t) \cos m\theta$ satisfies

$$\begin{aligned} v_{1t} &= \frac{1}{r} \frac{\partial}{\partial r} \left(r M(v_0) \frac{\partial \mathbf{m}_1}{\partial r} \right) - \frac{m^2}{r^2} M(v_0) \mathbf{m}_1, \\ \mathbf{m}_1 &= -\frac{\varepsilon^2}{r} \frac{\partial}{\partial r} \left(r \frac{\partial v_1}{\partial r} \right) + \left(\frac{m\varepsilon}{r} \right)^2 v_1 + f''(v_0) v_1, \end{aligned} \quad (73)$$

where $v_0(r)$ is the radially symmetric stationary state. We solve this system numerically, using the Chebyshev spectral collocation method (see Appendix) with $\Delta t = 10^{-3}$ and 400 mesh points until $t = 1/\varepsilon^2$. The decay rate of the eigenfunction is tracked by monitoring its maximum. The diffuse interface decay rates are scaled with $1/\varepsilon^2$ to compare with the sharp interface model. The base state that is needed for this calculation is determined *a priori* with the interface, *i.e.* the zero contour, positioned at $r_0 = 0.5$. The initial condition for the perturbation,

$$v_1(0, r) = \exp [1/(a^2 - (r_0 - r)^2)], \quad (74)$$

acts approximately as a shift to the leading order shape of the inner layer. The constant a is chosen so that the support of $v_1(0, r)$ lies in the range $r > r^*$.

The results are compared in Table 1. They show that the decay rate of the azimuthal perturbation to the radially symmetric base state obtained for $m = 2$ tends to the eigenvalue for the linearised sharp interface model *with* the contribution from nonlinear bulk diffusion, rather than to the one for pure surface diffusion. This confirms that (58) describes the leading order sharp interface evolution for the Cahn–Hilliard model (1) correctly, and that the sharp interface motion is distinct from the one induced by pure surface diffusion.

5 Modifications

5.1 Solutions with $u > 1$ for the mobility $M(u) = |1 - u^2|$

As pointed out in Section 3, solutions that have a modulus $|u| > 1$ and converge to the usual stationary Cahn–Hilliard solutions are conceivable for the mobility $M(u) = |1 - u^2|$ and are seen to arise in numerical solutions with this mobility for appropriate initial conditions. For this case, we can carry out the asymptotic derivations to obtain the sharp interface limit and match the inner problem to outer solutions on both sides of the interface, accepting thereby that the outer solution for u in Ω_+ is larger than one. Otherwise the detailed derivations follow the same pattern as in section 4.3 and can be found in [40].

ε	0.01	0.005	0.002	0.001	Eq (76)
$\lambda_{m=2}$	-144.7	-146.3	-147.5	-147.8	-148.1

Table 2: The decay rates of an azimuthal perturbation obtained by the diffuse and sharp interface models show good agreement for general initial condition not bounded between ± 1 and mobility $M(u) = 1 - u^2$. The numerical method and discretisation parameters are the same as in Table 1. The description of the numerical approach and parameters carries over from Table 1.

The upshot is that the sharp interface model now has contributions from nonlinear bulk diffusion on both sides of the interface, in addition to surface diffusion, *viz.*

$$\nabla \cdot (\mu_1^\pm \nabla \mu_1^\pm) = 0, \text{ on } \Omega_\pm, \quad (75a)$$

$$\mu_1^\pm = \frac{2}{3}\kappa, \text{ on } \zeta, \quad (75b)$$

$$\nabla_n \mu_1^+ = 0, \text{ on } \partial\Omega, \quad (75c)$$

$$v_n = \frac{2}{3}\partial_{ss}\kappa + \frac{1}{4}(\mu_1^+ \nabla_n \mu_1^+ + \mu_1^- \nabla_n \mu_1^-), \text{ on } \zeta. \quad (75d)$$

This sharp interface model predicts an exponential decay rate of

$$\lambda = -\frac{2}{3} \frac{m^2(m^2 - 1)}{r_0^4} - \frac{1}{9} \frac{m(m^2 - 1)}{r_0^4} (\tanh(m \log r_0^{-1}) + 1) \quad (76)$$

for the evolution of the perturbation to the radially symmetric stationary state with wave number m . Table 2 shows that equation (76) is indeed consistent with numerical results for the diffuse model. As a cautionary remark, we note that we are dealing here with a sign-changing solution of a degenerate fourth order problem, in the sense that $1 - u$ changes sign and the mobility degenerates. The theory for this type of problems is still being developed [25, 24, 4, 13, 11, 26].

5.2 Degenerate biquadratic mobility

For the mobilities investigated so far, nonlinear bulk diffusion enters at the same order as surface diffusion. If we employ $\tilde{M}(u) = ((1 - u^2)_+)^2$, then

$$j_2 = u_1 \tilde{M}'(u_0) \nabla_n \mu_1 = 0. \quad (77)$$

The contribution of the bulk diffusion flux to the normal velocity of the interface is subdominant to surface diffusion and therefore

$$v_n = \frac{1}{3} \int_{-\infty}^{\infty} \text{sech}^4 \rho \, d\rho \, \partial_{ss}\kappa = \frac{4}{9} \partial_{ss}\kappa. \quad (78)$$

Table 3 shows that the decay rate obtained from the numerical solution of the diffuse interface model for the degenerate biquadratic mobility is indeed consistent with the predictions obtained for the sharp interface model (78) with pure surface diffusion.

ε	0.01	0.005	0.001	Eq (71)
$\lambda_{m=2}$	-84.6	-84.7	-85.2	-85.3

Table 3: The decay rates obtained by the diffuse interface model for the mobility $M(u) = ((1 - u^2)_+)^2$ and $|u| < 1$ show good agreement with the surface diffusion model in (71), with $\mathfrak{M} = 4/9$, as $\varepsilon \rightarrow 0$. The description of the numerical approach and parameters carries over from table (1).

6 Conclusions

In this paper, we have derived the sharp interface limit for a Cahn–Hilliard model in two space dimensions with a nonlinear mobility $M(u) = (1 - u^2)_+$, and a double-well potential with minima at ± 1 for the homogeneous part of the free energy. We found that in addition to surface diffusion, there is also a contribution from bulk diffusion to the interface motion which enters at the same order. This contribution enters only from one side of the interface, whereas for the mobility $M(u) = |1 - u^2|$, solutions have also been considered for which bulk diffusion in the sharp interface limit enters from both sides at the same order as surface diffusion.

The situation studied here was focused on the case of convex $\Omega_+ = \{\mathbf{x} \in \Omega; u > 0\}$ with an $O(1)$ curvature for the interface $u = 0$, though the asymptotic analysis also remains valid if Ω_+ is the union of well-separated convex domains. The dynamics for concentric circles of different phases has also been looked into [40]. For the case where the interface has turning points, the derivation needs to be revisited, since the location of the free boundary Γ , given by $\rho = \sigma$ in inner coordinates about the interface, depends on the curvature so that $|\sigma| \rightarrow \infty$ if κ tends to zero. Moreover, as the curvature changes sign, Γ changes the side of the interface. On a different plane, it would also be interesting to investigate the coarsening behaviour [15] for the sharp interface model (58). For ensembles of two or more disconnected spheres, pure surface diffusion does not give rise to coarsening, but coarsening is expected for the mixed surface/bulk diffusion flux in (58).

While the Cahn–Hilliard equation (1) plays a role in some biological models, see for example [37], and may have significance in modelling spinodal decomposition in porous media, possibly with different combinations of mobilities, e.g. $M(u) = |1 - u^2| + \alpha(1 - u^2)^2$, see [40], the main motivation for our investigation stems from the role degenerate Cahn–Hilliard models play as a basis for numerical simulations for surface diffusion with interface motion driven by (2). The upshot for the specific combination of mobility and double well potential used in (1) is not useful for this purpose, since a contribution from bulk diffusion enters at the same order. For mobilities with higher degeneracy, such as $M(u) = ((1 - u^2)_+)^2$, this undesired effect is of higher order and can be made arbitrarily small, at least in principle, by reducing ε . Nevertheless, for finite ε , it is still present and a cumulative effect may arise for example through a small but persistent coarsening of phase-separated domains.

A range of alternatives can be found in the literature, in particular using the combi-

nation of $M = (1 - u^2)_+$ or $M = |1 - u^2|$ with the logarithmic or with the double obstacle potential [18]. These combinations force the order parameter u to be equal to or much closer to ± 1 away from the interface, thus shutting out the bulk diffusion more effectively. Numerical methods have been developed for these combinations and investigated in the literature, see for example [6, 9, 7, 8, 10, 27, 5]. Other approaches that have been suggested include a dependence of the mobility on the gradients of the order parameter [42], tensorial mobilities [33], or singular expressions for the chemical potential [50].

As a final remark, we note that many analytical questions remain open. For example, the existence of solutions that preserve the property that $|u| > 1$ in some parts of Ω has not been shown. Also, the approximation of (1) by a free boundary problem (3) should be investigated systematically using $b = \min(1 - |u|) > 0$ as a small parameter, in the spirit of what was done, for example, in [35] for the precursor model of a spreading droplet. The conditions at the free boundary Γ could then be recovered from matching to an inner solution. If $b \rightarrow 0$ in finite time, the effect of the “precursor” regularisation is lost and either the regularising effect implicit in the numerical discretisation or any explicit regularisation that is used (e.g., the one suggested in [23]) have to be taken into account. It would be interesting to see for which regularisations the conditions in (3c) are recovered. We note, however, that the evolution of the leading order sharp interface model in Ω_- is usually insensitive to the conditions imposed at Γ .

7 Appendix: Numerical Methods

We numerically solved the radially symmetric counterpart to (1) in polar coordinates without an explicit regularisation (such as the one used in [23]) via a Chebyshev spectral collocation method in space and semi-implicit time-stepping, using a linearised convex splitting scheme to treat f . For details on spectral methods in general, we refer the reader to the references [55, 56]. We also split the mobility as $M(u) \equiv (M(u) - \theta) + \theta$, to evaluate $(M(u) - \theta)$ at the previous time step whilst solving the remaining θ portion at the next time step, which improved the stability. We choose $\theta = 0.01\varepsilon$ in our simulations. Varying θ confirmed that the results did not sensitively depend on its value provided it was $O(\varepsilon)$.

As the Chebyshev–Lobatto points are scarcest in the middle of the domain, we resolve the interior layer by introducing a non-linear map $x \in [-1, 1] \mapsto r \in [0, 1]$, as suggested in [14], $r = (1/2) + \arctan(\delta \tan \pi x/2) / \pi$, where $0 < \delta < 1$ is a parameter that determines the degree of stretching of the interior domain, with a smaller value of δ corresponding to greater degree of localisation of mesh points about the centre of the domain. In this paper, we general set $\delta = 10\varepsilon$. This choice of δ is guided by numerical experiments, which show that further increase in the number of mesh points does not alter the stationary solution. Moreover, since $r = 0$ is a regular singular point, we additionally map the domain $r \in [0, 1]$ linearly onto a truncated domain $[10^{-10}, 1]$. Again, we verified that varying the truncation parameter did not affect the numerical results. Unless otherwise stated, the numerical simulations reported in the paper are done with 400 collocation points and timestep $\Delta t = 10^{-3}$.

The linearised phase-field models were solved using the same method, with a base state that was obtained from a preceding run and then “frozen” in time, *i.e.* not co-evolved with the perturbation.

References

- [1] H. Abels, H. Garcke, and G. Grün. Thermodynamically consistent, frame indifferent diffuse interface models for incompressible two-phase flows with different densities. *Mathematical Models and Methods in Applied Sciences*, 22(03):1150013, 2012.
- [2] H. Abels and M. Röger. Existence of weak solutions for a non-classical sharp interface model for a two-phase flow of viscous, incompressible fluids. *Annales de l’Institut Henri Poincaré (C) Non Linear Analysis*, 26(6):2403–2424, Nov. 2009.
- [3] N. D. Alikakos, P. W. Bates, and X. Chen. Convergence of the Cahn-Hilliard equation to the Hele-Shaw model. *Archive for Rational Mechanics and Analysis*, 128(2):165–205, 1994.
- [4] P. Alvarez-Caudevilla and V. A. Galaktionov. Well-posedness of the cauchy problem for a fourth-order thin film equation via regularization approaches. *arXiv:1311.0712 [math]*, Nov. 2013.
- [5] L. Banaš, A. Novick-Cohen, and R. Nürnberg. The degenerate and non-degenerate deep quench obstacle problem: A numerical comparison. *Networks and Heterogeneous Media*, 8(1):37–64, Mar. 2013.
- [6] J. W. Barrett and J. F. Blowey. Finite element approximation of a degenerate Allen–Cahn/Cahn–Hilliard system. *SIAM Journal on Numerical Analysis*, 39(5):1598–1624, Jan. 2002.
- [7] J. W. Barrett, J. F. Blowey, and H. Garcke. Finite element approximation of a fourth order nonlinear degenerate parabolic equation. *Numerische Mathematik*, 80(4):525–556, Oct. 1998.
- [8] J. W. Barrett, J. F. Blowey, and H. Garcke. Finite element approximation of the Cahn–Hilliard equation with degenerate mobility. *SIAM Journal on Numerical Analysis*, 37(1):286–318, Jan. 1999.
- [9] J. W. Barrett, J. F. Blowey, and H. Garcke. On fully practical finite element approximations of degenerate Cahn-Hilliard systems. *ESAIM: Mathematical Modelling and Numerical Analysis*, 35(4):713–748, Apr. 2002.
- [10] J. W. Barrett, H. Garcke, and R. Nürnberg. A phase field model for the electromigration of intergranular voids. *Interfaces and Free Boundaries*, 9:171–210, 2007.
- [11] F. Bernis. Finite speed of propagation and continuity of the interface for thin viscous flows. *Advances in Differential Equations*, 1(3):337–368, 1996.

- [12] D. N. Bhate, A. Kumar, and A. F. Bower. Diffuse interface model for electromigration and stress voiding. *Journal of Applied Physics*, 87(4):1712–1721, 2000.
- [13] M. Bowen and T. P. Witelski. The linear limit of the dipole problem for the thin film equation. *SIAM Journal on Applied Mathematics*, 66(5):1727–1748, May 2006.
- [14] J. P. Boyd. The arctan/tan and Kepler-Burgers mappings for periodic solutions with a shock, front, or internal boundary layer. *Journal of Computational Physics*, 98(2):181–193, 1992.
- [15] A. J. Bray and C. L. Emmott. Lifshitz-Slyozov scaling for late-stage coarsening with an order-parameter-dependent mobility. *Physical Review B*, 52(2):R685–R688, July 1995.
- [16] J. Cahn and J. Hilliard. Spinodal decomposition: A reprise. *Acta Metallurgica*, 19(2):151–161, Feb. 1971.
- [17] J. Cahn and J. Taylor. Surface motion by surface diffusion. *Acta Metallurgica et Materialia*, 42(4):1045–1063, Apr. 1994.
- [18] J. W. Cahn, C. M. Elliott, and A. Novick-Cohen. The Cahn-Hilliard equation with a concentration dependent mobility: motion by minus the laplacian of the mean curvature. *European Journal of Applied Mathematics*, 7(3):287–302, 1996.
- [19] J. W. Cahn and J. E. Hilliard. Free energy of a nonuniform system. i. interfacial free energy. *The Journal of Chemical Physics*, 28(2):258, 1958.
- [20] H. D. Ceniceros and C. J. García-Cervera. A new approach for the numerical solution of diffusion equations with variable and degenerate mobility. *Journal of Computational Physics*, 2013.
- [21] L. Chen. Phase-field models for microstructure evolution. *Annual review of materials research*, 32(1):113–140, 2002.
- [22] S. Dai and Q. Du. Motion of interfaces governed by the Cahn–Hilliard Equation with highly disparate diffusion mobility. *SIAM Journal on Applied Mathematics*, 72(6):1818–1841, Nov. 2012.
- [23] C. M. Elliott and H. Garcke. On the Cahn-Hilliard equation with degenerate mobility. *SIAM Journal on Mathematical Analysis*, 27(2):404–423, 1996.
- [24] J. D. Evans, V. A. Galaktionov, and J. R. King. Source-type solutions of the fourth-order unstable thin film equation. *European Journal of Applied Mathematics*, 18(3):273–321, 2007.
- [25] V. A. Galaktionov. Very singular solutions for thin film equations with absorption. *Studies in Applied Mathematics*, 124(1):39–63, 2010.

- [26] V. A. Galaktionov. On Oscillations of Solutions of the Fourth-Order Thin Film Equation Near Heteroclinic Bifurcation Point. *arXiv:1312.2762 [math]*, 2013.
- [27] H. Garcke, R. Nürnberg, and V. Styles. Stress- and diffusion-induced interface motion: Modelling and numerical simulations. *European Journal of Applied Mathematics*, 18(6):631–657, 2007.
- [28] G. Giacomin and J. L. Lebowitz. Exact macroscopic description of phase segregation in model alloys with long range interactions. *Physical Review Letters*, 76(7):1094, 1996.
- [29] G. Giacomin and J. L. Lebowitz. Phase segregation dynamics in particle systems with long range interactions I: Macroscopic limits. *Journal of Statistical Physics*, 87(1-2):37–61, 1997.
- [30] G. Giacomin and J. L. Lebowitz. Phase segregation dynamics in particle systems with long range interactions II: Interface motion. *SIAM Journal on Applied Mathematics*, 58(6):1707–1729, 1998.
- [31] G. Giacomin, J. L. Lebowitz, and R. Marra. Macroscopic evolution of particle systems with short-and long-range interactions. *Nonlinearity*, 13(6):2143, 2000.
- [32] K. Glasner. A diffuse interface approach to Hele–Shaw flow. *Nonlinearity*, 16(1):49, 2003.
- [33] C. Gugenberger, R. Spatschek, and K. Kassner. Comparison of phase-field models for surface diffusion. *Physical Review E*, 78(1):016703, 2008.
- [34] W. Jiang, W. Bao, C. V. Thompson, and D. J. Srolovitz. Phase field approach for simulating solid-state dewetting problems. *Acta Materialia*, 60(15):5578–5592, 2012.
- [35] J. R. King and M. Bowen. Moving boundary problems and non-uniqueness for the thin film equation. *European Journal of Applied Mathematics*, 12(03):321–356, 2001.
- [36] K. Kitahara and M. Imada. On the kinetic equations for binary mixtures. *Progress in Theoretical Physics Supplement*, 64:65–73, 1978.
- [37] I. Klapper and J. Dockery. Role of cohesion in the material description of biofilms. *Physical Review E*, 74(3), Sept. 2006.
- [38] M. D. Korzec, P. L. Evans, A. Münch, and B. Wagner. Stationary solutions of driven fourth-and sixth-order Cahn-Hilliard-type equations. *SIAM Journal on Applied Mathematics*, 69(2):348–374, 2008.
- [39] C. G. Lange. On spurious solutions of singular perturbation problems. *Studies in Applied Mathematics*, 68:227–257, 1983.
- [40] A. A. Lee. On the Sharp Interface Limits of the Cahn-Hilliard Equation. M.Sc. thesis, University of Oxford, 2013.

- [41] H.-W. Lu, K. Glasner, A. L. Bertozzi, and C.-J. Kim. A diffuse-interface model for electrowetting drops in a hele-shaw cell. *Journal of Fluid Mechanics*, 590:411–435, 2007.
- [42] M. Mahadevan and R. M. Bradley. Phase field model of surface electromigration in single crystal metal thin films. *Physica D: Nonlinear Phenomena*, 126(3):201–213, 1999.
- [43] W. W. Mullins. Theory of thermal grooving. *Journal of Applied Physics*, 28:333, 1957.
- [44] W. W. Mullins and R. F. Sekerka. Morphological stability of a particle growing by diffusion or heat flow. *Journal of Applied Physics*, 34(2):323–329, 1963.
- [45] B. S. Niethammer. Existence and uniqueness of radially symmetric stationary points within the gradient theory of phase transitions. *European Journal of Applied Mathematics*, 6(01), Feb. 1995.
- [46] R. L. Pego. Front migration in the nonlinear Cahn-Hilliard equation. *Proceedings of the Royal Society of London. A. Mathematical and Physical Sciences*, 422(1863):261–278, 1989.
- [47] N. Provatas and K. Elder. *Phase-field methods in materials science and engineering*. Wiley Interscience, 2010.
- [48] S. Puri, A. J. Bray, and J. L. Lebowitz. Phase-separation kinetics in a model with order-parameter-dependent mobility. *Physical Review E*, 56(1):758–765, July 1997.
- [49] A. Rätz, A. Ribalta, and A. Voigt. Surface evolution of elastically stressed films under deposition by a diffuse interface model. *Journal of Computational Physics*, 214(1):187–208, 2006.
- [50] A. Rätz, A. Ribalta, and A. Voigt. Surface evolution of elastically stressed films under deposition by a diffuse interface model. *Journal of Computational Physics*, 214(1):187–208, May 2006.
- [51] D. N. Sibley, A. Nold, and S. Kalliadasis. Unifying binary fluid diffuse-interface models in the sharp-interface limit. *Journal of Fluid Mechanics*, 736:5–43, 2013.
- [52] J. E. Taylor and J. W. Cahn. Linking anisotropic sharp and diffuse surface motion laws via gradient flows. *Journal of Statistical Physics*, 77(1-2):183–197, Oct. 1994.
- [53] S. Torabi and J. Lowengrub. Simulating interfacial anisotropy in thin-film growth using an extended cahn-hilliard model. *Physical Review E*, 85(4):041603, Apr. 2012.
- [54] S. Torabi, J. Lowengrub, A. Voigt, and S. Wise. A new phase-field model for strongly anisotropic systems. *Proceedings of the Royal Society A: Mathematical, Physical and Engineering Science*, 465(2105):1337–1359, May 2009.

- [55] L. N. Trefethen. *Spectral methods in MATLAB*, volume 10. SIAM, 2000.
- [56] L. N. Trefethen. *Approximation theory and approximation practice*. SIAM, 2013.
- [57] S. van Gemmert, G. T. Barkema, and S. Puri. Phase separation driven by surface diffusion: A monte carlo study. *Physical Review E*, 72(4):046131, Oct. 2005.
- [58] J. K. Wolterink, G. T. Barkema, and S. Puri. Spinodal decomposition via surface diffusion in polymer mixtures. *Physical Review E*, 74(1):011804, July 2006.